Hindawi
Shock and Vibration
Volume 2018, Article ID 5017564, 15 pages
https://doi.org/10.1155/2018/5017564

Research Article

Hierarchical Modeling and Dynamic Analysis of Hoist System in Electric Mining Shovel

Wei Sun, Jianan Du, Lintao Wang, Penglong Luan, and Jie li

School of Mechanical Engineering, Dalian University of Technology, Dalian 116024, China

Correspondence should be addressed to Lintao Wang; wlt@dlut.edu.cn

Received 15 May 2018; Revised 18 July 2018; Accepted 2 August 2018; Published 13 September 2018

Academic Editor: Shuaishuai Sun

The hoist system of electric mining shovel (EMS) always encounters excessive vibration in present work. However, the shortage of suitable dynamic model has been the bottleneck of reducing vibration. In order to analyze the vibration of the EMS hoist system, a coupled dynamic model is proposed using the hierarchical modeling method, which contains couplings of bolt, bear, coupling, rope, and gear mesh. The components were equivalent to mass elements with several nodes corresponding to their structure. Considered helical gears and motors, a dynamic gear transmission model with couplings of bending, torsion, and axes was developed. Based on the dynamic model, the modal characteristics were calculated, and the vibration modes were classified to five types. Under the ripple drive torque simulated by Simulink, the dynamic characteristics of the hoist system in time domain and frequency domain were obtained using numerical integration with the Runge–Kutta method in Matlab. At last, the model validity was verified by contrasting the responses under actual test and the model. The dynamic model and study results can provide support for dynamic characteristic evaluation and dynamic optimization of the EMS hoist system.

1. Introduction

Electric mining shovel (EMS) is a large engineering machine widely used in open pit mine for excavating and loading the blasted material onto the mining dump truck. Its dipper capacity can reach as high as 75 m^3.

Hoist system is one of the key subsystems of EMS. During excavating process, it cooperates with the crowd system (another subsystem of EMS) to push the dipper and bucket arm for excavating material. The hoist system is a complex nonlinear system, which mainly consists of driving motors, multistage gear transmission system, and flexible ropes. The multistage gear transmission system is a strong coupling system which causes periodic excitation owing to the nonlinear factors such as time-varying mesh stiffness, transmission error, and backlash [1]. As a result of inadequately blasted ores [2] and unskilled workers [3], the hoist system often suffers large impact load with drastic fluctuation during practical operation [4]. Under such internal excitation formed in gear transmission system and external excitation caused by geological condition and converter motor, server vibration in the hoist system often occurs and results in components failure [5].

Actually, most failures of a machine can be avoided effectively via rational design [6]. In designing such a large EMS, modeling approach and the simulation model are of vital importance since experiments are nearly impossible in design stage. In recent years, some research studies have been done on developing simulation model or virtual prototype of EMS. Li et al. obtained the force of every component under different conditions by simulation in ADAMS [7]. Khorzoughi et al. analyzed the vibration of hoist rope under different digging conditions and found that the vibration amplitude was related to the digging force [8]. Guzmán and Valenzuela presented an integrated model of the shovel containing simple mechanical system and vector control motor system, where the shovel is modeled as a 4-DOF mechanical system with three rotating joints and one prismatic joint. From the model, every force in the joint and parameters about driving motor can be contained all the time [9]. However, the existing research studies are mainly focused on developing simple models of whole system concerning force transmission but hardly related to the dynamic properties of its components. These models cannot be applied in dynamic analysis and design of the hoist system.

As the critical components of hoist system, reducer gears are also the maximum failure rate part. Therefore, the dynamic properties of the gear transmission system need to be especially considered. Wei et al. studied the dynamic characteristics of multigear drive system in tunnel boring machine and then found that the maximum dynamic load with the influence of bending-torsional coupling is greater than that without the influence of bending-torsional coupling [10, 11]. Qin et al. developed a mathematical model of horizontal wind turbine drivetrain and analyzed its vibration modes, and results revealed that the vibration modes of planetary gear as a subsystem in drivetrain are different from being stand-alone [12]. Sun et al. compared the dynamic responses of TBM cutter-head system under ideal torque and actual electromagnetic torque, and results showed that the vibration displacements of gears are aggravated owing to the torque ripple [13]. Indicated by the above research studies, the dynamic behaviors of the gear transmission system are closely related to the connected components. Therefore, for analyzing the dynamic response of the hoist system exactly, all the connected and coupled components must be considered in modeling process.

Motivated by the above observations, this paper is mainly focused on dynamic modeling and analysis of the hoist system in EMS. The main contribution of this paper includes the following: (1) a electromechanical coupling dynamic model including mechanical and control system was established based on hierarchical modeling method and verified its validity. Both the subsystems of EMS and the couplings among subsystems, i.e., bolt connection and spline connection, gear mesh, and flexible coupling connection were integrated and considered in this model. (2) Vibration modes, displacement, and acceleration responses were calculated and evaluated. This information could be used in dynamic design of the hoist system in order to prevent premature failure as a result of excessive vibration.

2. Hierarchical Modeling of Hoist System

The structure of EMS hoist system is shown in Figure 1, which is mainly composed of motors, reducer, drum, rope, boom, and dipper. During the hoist process, hoist force provided by hoist motors is transported from reducer and drum to rope, and then the dipper is controlled by the rope.

Obviously, the EMS hoist system can be seen as an integrated system consisting of several subsystems and components with couplings such as flexible coupling connection, gear mesh, bolt connection, bearing connection, and coupling connection. It is suitable to establish the EMS hoist system model using the hierarchical theory [14]. The hoist system can be divided into several subsystems according to their coupling relationships.

Taking the EMS with standard dipper capacity of 55 m^3 as an example, the modeling process of the hoist system using hierarchical way is shown in Figure 2. Firstly, the hoist system can be divided into mechanical system and control system in physics [15]. The mechanical system can be split into three subsystems including reducer shell subsystem, gear subsystem, and rope subsystem. During modeling process, the reducer shell, drum, and boom are equivalent to mass element with different number of nodes. The dynamic model of gear subsystem is established using the lumped mass method. The connections such as coupling, bolt, and bearing are equivalent to spring-damper elements. As for the control system, the hoist motor uses variable frequency speed control (VFSC). To be exact, the example equipment takes vector control (VC) as control strategy. With the connections of coupling, bolt, and bearing, the model of the EMS hoist system can be coupled by the four subsystems.

2.1. Dynamic Model of Mechanical System. The dynamic model of the mechanical system is shown in Figure 3. The node number and corresponding force of each component is determined by its structure features and connection relations.

2.1.1. Dynamic Model of Reducer Shell Subsystem. Reducer shell subsystem consists of the reducer shell and the base. Taking the reducer shell as a rigid body of two nodes and every node has three freedoms in direction x, y, and z, the reducer shell has six freedoms. The dynamic model of reducer shell subsystem is shown in Figure 4. Where o_1 and o_2 are the locations' installed bolts; o_3, o_4, o_6, and o_7 are the axis of input shaft and intermediate shaft on both sides.

The force is transformed from gear shafts and bearings to reducer shell. Setting the mass of the reducer shell is divided into two nodes equally, and the equivalent mathematic model of reducer shell can be expressed as follows:

$$
\begin{aligned}
\ddot{x}_1 &= \frac{(F_{6kc}+F_{7kc}-F_{3kc}-F_{4kc})\sin\theta-(k_{1x}+k_{2x})x_1-(c_{1x}+c_{2x})\dot{x}_1}{m_1+m_2},\\
\ddot{y}_1 &= \frac{(F_{3kc}(l_3+l_4)\cos\theta+2l_3(F_{4kc}\cos\theta+F_{5kc})+F_{10kc}l_3-F_{6kc}(l_4+l_3)\cos\theta-2(F_{3kc}l_1+F_{4kc}l_2)\sin\theta+2(F_{6kc}l_1+F_{7kc}l_2)\sin\theta)/(2l_3)-k_{1y}y_1-c_{1y}\dot{y}_1}{m_1},\\
\ddot{z}_1 &= \frac{(F_{3z}(l_3+l_4)+2F_{4z}l_3+F_{10z}l_3-F_{6z}(l_4-l_3))/(2l_3)-k_{1z}z_1-c_{1z}\dot{z}_1}{m_1},\\
\ddot{x}_2 &= \frac{(F_{6kc}+F_{7kc}-F_{3kc}-F_{4kc})\sin\theta-(k_{1x}+k_{2x})x_2-(c_{1x}+c_{2x})\dot{x}_2}{m_1+m_2},\\
\ddot{y}_2 &= \frac{(F_{3kc}(l_4-l_3)\cos\theta-F_{10kc}l_3-2(F_{7kc}\cos\theta+F_{8kc})l_3-F_{6kc}(l_3+l_4)\cos\theta-2(F_{3kc}l_1+F_{4kc}l_2)\sin\theta+2(F_{6kc}l_1+F_{7kc}l_2)\sin\theta)/(2l_3)-k_{2y}y_2-c_{2y}\dot{y}_2}{m_2},\\
\ddot{z}_2 &= \frac{(F_{6z}(l_3+l_4)+2F_{7z}l_3+F_{10z}l_3-F_{3z}(l_4-l_3))/(2l_3)-k_{2z}z_2-c_{2z}\dot{z}_2}{m_2},
\end{aligned}
\tag{1}
$$

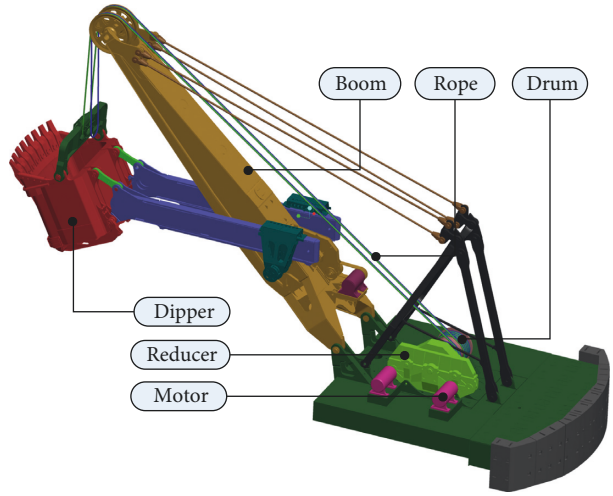

Figure 1: Structure diagram of EMS hoist system.

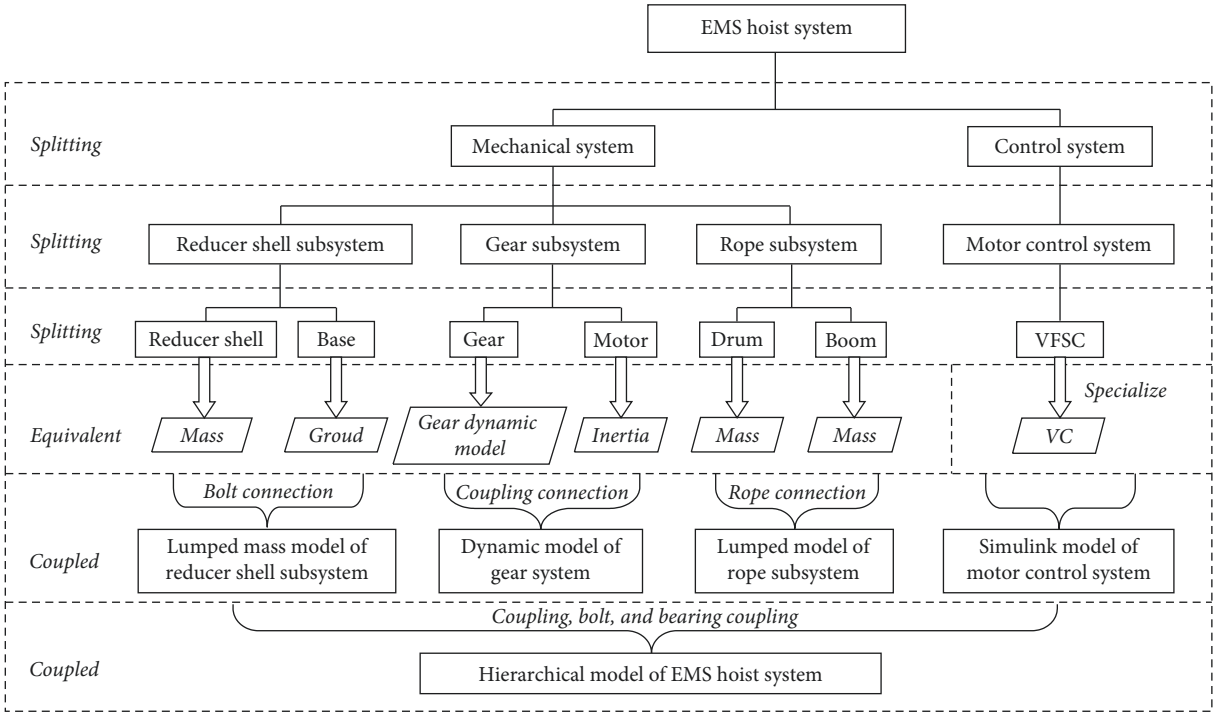

Figure 2: Hierarchical modeling flow of the EMS hoist system.

where m_1, m_2 are the mass of node 1 and node 2; $x_1, y_1, z_1, x_2, y_2, z_2$ are displacement of nodes 1 and 2; θ is the included angle of vertical and direction perpendicular to the line connecting o_3 and o_4 or o_6 and o_7; $k_{1x}, k_{1y}, k_{1z}, k_{2x}, k_{2y}, k_{2z}$ are the stiffness of bolts located in nodes 1 and 2; $c_{1x}, c_{1y}, c_{1z}, c_{2x}, c_{2y}, c_{2z}$ are the damping of bolts located in nodes 1 and 2; and l_1, l_2, l_3, l_4 are the length from o_6 to o_2, o_7 to o_2, o_1 to o_2, o_3 to o_6.

$F_{3kc}, F_{4kc}, F_{5kc}, F_{6kc}, F_{7kc}, F_{8kc}, F_{10kc}$ are the force transformed from different gears and gear shafts to reducer shell in x-y plane; $F_{3z}, F_{4z}, F_{6z}, F_{7z}, F_{10z}$ are the forces transformed from different gears, gear shafts, or the drum to reducer shell in y-z plane. They can be calculated according to

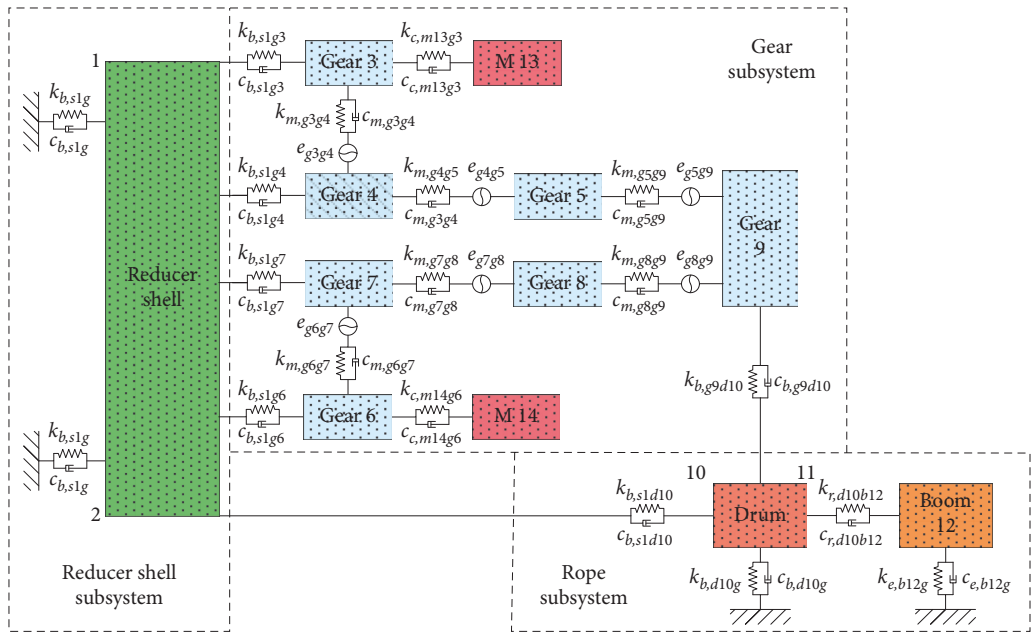

Figure 3: Dynamic model of mechanical system.

$$
\begin{aligned}
F_{3kc} &= k_{3y}(y_3 - y_3') + c_{3y}(\dot{y}_3 - \dot{y}_3'),\\
F_{4kc} &= k_{4y}(y_4 - y_4') + c_{4y}(\dot{y}_4 - \dot{y}_4'),\\
F_{5kc} &= k_{5y}(y_5 - y_5') + c_{5y}(\dot{y}_5 - \dot{y}_5'),\\
F_{6kc} &= k_{6y}(y_6 - y_6') + c_{6y}(\dot{y}_6 - \dot{y}_6'),\\
F_{7kc} &= k_{7y}(y_7 - y_7') + c_{7y}(\dot{y}_7 - \dot{y}_7'),\\
F_{8kc} &= k_{8y}(y_8 - y_8') + c_{8y}(\dot{y}_8 - \dot{y}_8'),\\
F_{10kc} &= k_{10y}(y_{10} - y_{10}') + c_{10y}(\dot{y}_{10} - \dot{y}_{10}'),\\
F_{3z} &= k_{3z}\left(z_3 - \left(z_1 + \frac{z_1 - z_2}{l_3}\frac{l_4 - l_3}{2}\right)\right)\\
&\quad + c_{3z}\left(\dot{z}_3 - \left(\dot{z}_1 + \frac{\dot{z}_1 - \dot{z}_2}{l_3}\frac{l_4 - l_3}{2}\right)\right),\\
F_{4z} &= k_{4z}(z_4 - z_1) + c_{4z}(\dot{z}_4 - \dot{z}_1),\\
F_{6z} &= k_{6z}\left(z_6 - \left(z_1 - \frac{z_1 - z_2}{l_3}\frac{l_4 + l_3}{2}\right)\right)\\
&\quad + c_{6z}\left(\dot{z}_6 - \left(\dot{z}_1 - \frac{\dot{z}_1 - \dot{z}_2}{l_3}\frac{l_4 + l_3}{2}\right)\right),\\
F_{7z} &= k_{7z}(z_7 - z_2) + c_{7z}(\dot{z}_7 - \dot{z}_2),\\
F_{10z} &= k_{10z}\left(z_{10} - \frac{z_1 + z_2}{2}\right) + c_{10z}\left(\dot{z}_{10} - \frac{\dot{z}_1 + \dot{z}_2}{2}\right),
\end{aligned}
\tag{2}
$$

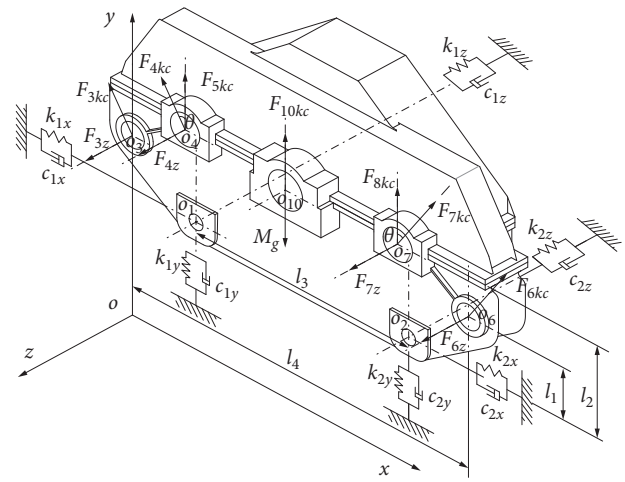

Figure 4: Dynamic model of reducer shell subsystem.

where $k_{3y}, k_{4y}, k_{5y}, k_{6y}, k_{7y}, k_{8y}, k_{10y}$ are the brace stiffness of bearing in x-y plane; $k_{3z}, k_{4z}, k_{6z}, k_{7z}, k_{10z}$ are the brace stiffness of bearing in direction z; $c_{3y}, c_{4y}, c_{5y}, c_{6y}, c_{7y}, c_{8y}, c_{10y}$ are the equivalent damping of bearing in x-y plane; $c_{3z}, c_{4z}, c_{6z}, c_{7z}, c_{10y}$ are the equivalent damping of bearing in direction z; $y_3, y_4, y_5, y_6, y_7, y_8, y_{10}, z_3, z_4, z_6, z_7, z_{10}$ are the displacement of every gears and drum shown in Figures 5 and 6; and $y_3', y_4', y_5', y_6', y_7', y_8', y_9', y_{10}'$ are the displacement of point $o_3, o_4, o_4, o_6, o_7, o_7, o_{10}$ in same direction to $y_3, y_4, y_5, y_6, y_7, y_8, y_{10}$.

2.1.2. Dynamic Model of Gear Subsystem. There are seven gears and two motors in gear subsystem which has double input torques and single output torque. The first stage deceleration is helical gear transmission and the second is spur

gear transmission in gear subsystem. Using the lumped mass method, the dynamic model of gear subsystem can be presented with a bend-torsion-axes gear rotor model as shown in Figure 5 [16], where o_{13}, o_{14} are rotational centers of motor and $o_{g3}, o_{g4}, o_{g5}, o_{g6}, o_{g7}, o_{g8}, o_{g9}$ are gear centers. Ignoring the friction of gear tooth surface, the whole system has 2 rotational freedoms with two motors and 21 freedoms with seven gears. The equivalent mathematical model of gear subsystem can be expressed as follows:

$$
\begin{aligned}
J_3\ddot{\varphi}_3 &= k_{1303}(\varphi_{13}-\varphi_3)+c_{1303}(\dot{\varphi}_{13}-\dot{\varphi}_3)+r_3F_{34y},\\
m_3\ddot{y}_3 &= -k_{3y}(y_3-y_3')-c_{3y}(\dot{y}_3'-\dot{y}_3')-F_{34y},\\
m_3\ddot{z}_3 &= -k_{3z}(z_3-z_3')-c_{3z}(\dot{z}_3-\dot{z}_3')+F_{34z},\\
J_4\ddot{\varphi}_4 &= -k_{0405}(\varphi_4-\varphi_5)-c_{0405}(\dot{\varphi}_4-\dot{\varphi}_5)-r_4F_{34y},\\
m_4\ddot{y}_4 &= -k_{4y}(y_4-y_4')-c_{4y}(\dot{y}_4-\dot{y}_4')+F_{34y},\\
(m_4+m_5)\ddot{z}_4 &= -k_{4z}(z_4-z_4')-c_{4z}(\dot{z}_4-\dot{z}_4')-F_{34z},\\
J_5\ddot{\varphi}_5 &= k_{0405}(\varphi_4-\varphi_5)+c_{0405}(\dot{\varphi}_4-\dot{\varphi}_5)-r_5F_{59},\\
m_5\ddot{y}_5 &= -k_{5y}(y_5-y_5')-c_{5y}(\dot{y}_5-\dot{y}_5')-F_{59y},\\
(m_4+m_5)\ddot{z}_5 &= -k_{5z}(z_5-z_5')-c_{5z}(\dot{z}_5-\dot{z}_5')-F_{34z},\\
J_6\ddot{\varphi}_6 &= k_{1406}(\varphi_{14}-\varphi_6)+c_{1406}(\dot{\varphi}_{14}-\dot{\varphi}_6)+r_6F_{67y},\\
m_6\ddot{y}_6 &= -k_{6y}(y_6-y_6')-c_{6y}(\dot{y}_6-\dot{y}_6')-F_{67y},\\
m_6\ddot{z}_6 &= -k_{6z}(z_6-z_6')-c_{6z}(\dot{z}_6-\dot{z}_6')+F_{67z},\\
J_7\ddot{\varphi}_7 &= -k_{0708}(\varphi_7-\varphi_8)-c_{0708}(\dot{\varphi}_7-\dot{\varphi}_8)-r_7F_{67y},\\
m_7\ddot{y}_7 &= -k_{7y}(y_7-y_7')-c_{7y}(\dot{y}_7-\dot{y}_7')+F_{67y},\\
(m_7+m_8)\ddot{z}_7 &= -k_{7z}(z_7-z_7')-c_{7z}(\dot{z}_7-\dot{z}_7')-F_{67z},\\
J_8\ddot{\varphi}_8 &= k_{0708}(\varphi_7-\varphi_8)+c_{0708}(\dot{\varphi}_7-\dot{\varphi}_8)-r_8F_{98},\\
m_8\ddot{y}_8 &= -k_{08y}(y_8-y_8')-c_{8y}(\dot{y}_8-\dot{y}_8')+F_{98},\\
(m_7+m_8)\ddot{z}_8 &= -k_{8z}(z_8-z_8')-c_{8z}(\dot{z}_8-\dot{z}_8')-F_{67z},\\
J_9\ddot{\varphi}_9 &= -k_{0910}(\varphi_9-\varphi_{10})-c_{0910}(\dot{\varphi}_9-\dot{\varphi}_{10})+r_9F_{59}\\
&\quad +r_9F_{98},\\
m_9\ddot{y}_9 &= -k_{9y}(y_9-y_{10})-c_{9y}(\dot{y}_9-\dot{y}_{10})+F_{59}-F_{98},\\
m_9\ddot{z}_9 &= -k_{9z}(z_9-z_{10})-c_{9z}(\dot{z}_9-\dot{z}_{10}),\\
J_{13}\ddot{\varphi}_{13} &= -k_{1303}(\varphi_{13}-\varphi_3)-c_{1303}(\dot{\varphi}_{13}-\dot{\varphi}_3)+T_{\mathrm{e}},\\
J_{14}\ddot{\varphi}_{14} &= -k_{1406}(\varphi_{14}-\varphi_6)-c_{1406}(\dot{\varphi}_{14}-\dot{\varphi}_6)+T_{\mathrm{e}},
\end{aligned}
\tag{3}
$$

where $J_3, J_4, J_5, J_6, J_7, J_8, J_9, J_{13}, J_{14}$ are inertia moment of gears 3, 4, 5, 6, 7, 8, and 9 and motors 13 and 14; $m_3, m_4, m_5, m_6, m_7, m_8, m_9$ are mass of gear 3 plus input shaft, gear 4 plus half of intermediate shaft, gear 5 plus half of intermediate shaft, gear 6 plus input shaft, gear 7 plus half of intermediate shaft, gear 8 plus half of intermediate shaft, and gear 9; $\varphi_3, \varphi_4, \varphi_5, \varphi_6, \varphi_7, \varphi_8, \varphi_9, \varphi_{13}, \varphi_{14}$ are the rotational angles of gears 3, 4, 5, 6, 7, 8, and 9 and motors 13 and 14; z_5, z_8, z_9, y_9 are displacements of gears 5, 8, 9; k_{1303}, k_{1406} are torsional stiffness of couplings, k_{0405}, k_{0708} are torsional stiffness of intermediate shafts, and k_{0910} is torsional stiffness of bolts; k_{5z}, k_{8z} are the brace stiffness of bearing and k_{9y}, k_{9z} are equivalent stiffness of bolts; c_{1303} and c_{1406} are the equivalent rotary dampings of couplings, c_{0405} and c_{0708} are the equivalent rotary dampings of intermediate shafts, and c_{0910} is the equivalent rotary damping of bolts; $c_{4z}, c_{5z}, c_{7z}, c_{8z}$ are equivalent dampings of bearings; c_{9y}, c_{9z} are equivalent dampings of bolts; $r_3, r_4, r_5, r_6, r_7, r_8, r_9$ are the base radii of gears 3, 4, 5, 6, 7, 8, and 9; and T_{e} is the driving torque.

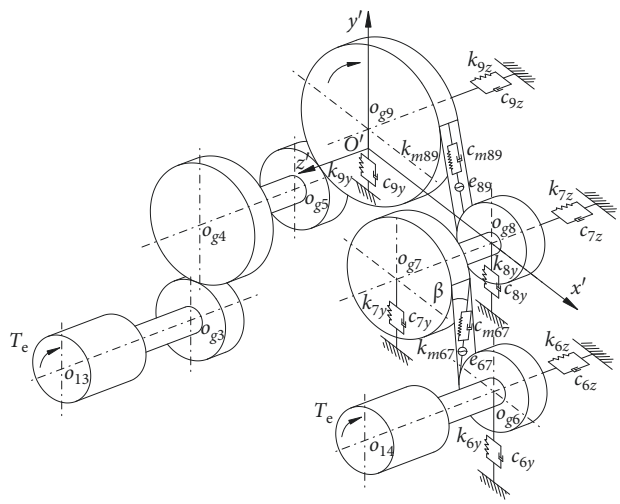

Figure 5: Dynamic model of gear subsystem.

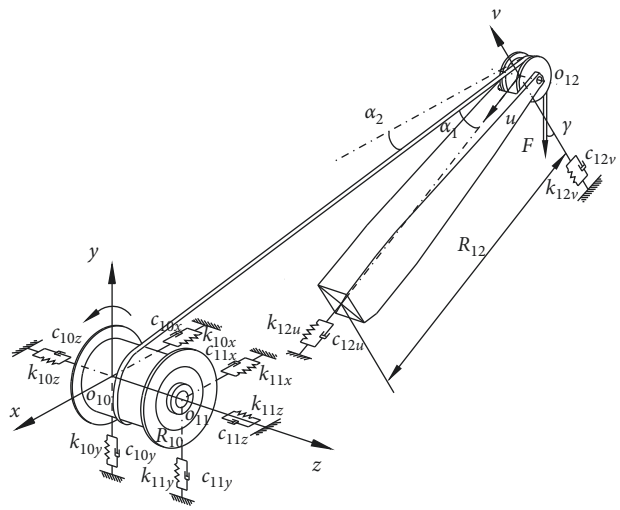

Figure 6: Dynamic model of rope subsystem.

F_{34y}, F_{34z} are dynamic mesh forces of gears 3 and 4; F_{67y}, F_{67z} are dynamic mesh forces of gears 6 and 7; F_{59} is dynamic mesh force of gears 5 and 9; and F_{98} is dynamic mesh force of gears 8 and 9. Mesh forces can be calculated by the following equation:

$$
\begin{aligned}
F_{34y} &= \cos\beta\left(k_{m34}\left(y_3-\varphi_3 r_3-y_4+\varphi_4 r_4-e_{34}\right)\right.\\
&\quad\left.+c_{m34}\left(\dot{y}_3-\dot{\varphi}_3 r_3-\dot{y}_4+\dot{\varphi}_4 r_4-\dot{e}_{34}\right)\right),\\
F_{34z} &= \sin\beta\left(k_{m34}\left(z_3-\left(y_3-\varphi_3 r_3\right)\tan\beta-z_4\right.\right.\\
&\quad\left.+\left(y_4-\varphi_4 r_4\right)\tan\beta-e_{34}\right)+c_{m34}\left(\dot{z}_3-\left(\dot{y}_3-\dot{\varphi}_3 r_3\right)\tan\beta\right.\\
&\quad\left.\left.-\dot{z}_4+\left(\dot{y}_4-\dot{\varphi}_4 r_4\right)\tan\beta-\dot{e}_{34}\right)\right),\\
F_{59} &= k_{m59}\left(y_5+\varphi_5 r_5-y_9-\varphi_9 r_9-e_{59}\right)\\
&\quad+c_{m59}\left(\dot{y}_5+\dot{\varphi}_5 r_5-\dot{y}_9-\dot{\varphi}_9 r_9-\dot{e}_{59}\right),\\
F_{67y} &= \cos\beta\left(k_{m67}\left(y_6+\varphi_6 r_6-y_7-\varphi_7 r_7-e_{67}\right)\right.\\
&\quad\left.+c_{m34}\left(\dot{y}_6+\dot{\varphi}_6 r_6-\dot{y}_7-\dot{\varphi}_7 r_7-\dot{e}_{67}\right)\right),\\
F_{67z} &= \sin\beta\left(k_{m67}\left(z_6-\left(y_6+\varphi_6 r_6\right)\tan\beta-z_7\right.\right.\\
&\quad\left.+\left(y_7+\varphi_7 r_7\right)\tan\beta-e_{67}\right)+c_{m34}\left(\dot{z}_6-\left(\dot{y}_6+\dot{\varphi}_6 r_6\right)\tan\beta\right.\\
&\quad\left.\left.-\dot{z}_7+\left(\dot{y}_7+\dot{\varphi}_7 r_7\right)\tan\beta-\dot{e}_{67}\right)\right),\\
F_{98} &= k_{m89}\left(y_9-\varphi_9 r_9-y_8+\varphi_9 r_9-e_{89}\right)\\
&\quad+c_{m59}\left(\dot{y}_5+\dot{\varphi}_5 r_5-\dot{y}_9-\dot{\varphi}_9 r_9-\dot{e}_{89}\right),
\end{aligned}
\tag{4}
$$

where β is the helical angle of helical gear.

$k_{m34}, k_{m59}, k_{m67}, k_{m89}$ are time-varying mesh stiffness of gears 3 and 4, gears 5 and 9, gears 6 and 7, and gears 8 and 9, which can be expressed by means of the Fourier series expansion as follows [17]:

$$
k_m(t) = k_0 + \sum_{i=1}^{n} k_i \cos\left(i\omega_m t + \phi_i\right), \tag{5}
$$

where k_0 is the average meshing stiffness which can be obtained based on gear standards AGMA ISO 1328-1; ω_m is the mesh frequency; ϕ_i is the meshing phase angle; and k_i is the n-rank harmonic amplitude in Fourier series.

$e_{34}, e_{59}, e_{67}, e_{89}$ are time-varying transmission errors which can be approximated as the superposition of the harmonic function of shaft frequency and meshing frequency [18], which can be expressed by the following equation:

$$
e(t) = 0.5F_{\mathrm{p}} \sin\left(2\pi\omega_{\mathrm{f}} t + \varphi_{\mathrm{f}}\right) + 0.5 f_i' \sin\left(2\pi\omega_m t + \varphi_m\right), \tag{6}
$$

where F_{p} is the cumulative tolerance of tooth distance; f_i' is the tangential tolerance of single tooth; ω_{f} is shaft frequency; and $\varphi_{\mathrm{f}}, \varphi_m$ are initial phases of shaft and mesh.

$c_{m34}, c_{m59}, c_{m67}, c_{m89}$ are dampings of gear mesh in gears 3 and 4, gears 5 and 9, gears 6 and 7, and gears 8 and 9, which can be calculated as follows [19]:

$$
c_m = 2\xi_{\mathrm{g}} \sqrt{\frac{k_0 r_{\mathrm{p}}^2 r_{\mathrm{g}}^2 I_{\mathrm{p}} I_{\mathrm{g}}}{r_{\mathrm{p}}^2 I_{\mathrm{p}} + r_{\mathrm{g}}^2 I_{\mathrm{g}}}}, \tag{7}
$$

where ξ_{g} is the damping ratio of gear mesh, which is between 0.03 and 0.17; r_{p} and r_{g} are base radii of gears; I_{p} and I_{g} are moment of inertia of gears.

2.1.3. Dynamic Model of Rope Subsystem. Rope subsystem is made up of drum and boom which are connected by steel ropes. One side of hoist drum is assembled with reducer shell, and the other side is fixed on the base. Equivalent to mass component with two nodes, the drum has six liner freedoms and one rotational freedom. Connected to the base in bottom and pulled by suspension rope in top, the boom can rotate around the pin roll. Hence, the boom can be equivalent to mass component with two freedoms, i.e., one is along the boom direction and the other is rotating around the pin roll. As for the steel rope, it can be equivalent to a spring element. As shown in Figure 6, the equivalent dynamic model of rope subsystem can be established as follows:

$$
\begin{aligned}
\ddot{\varphi}_{10} &= \frac{k_{0910}\left(\varphi_9-\varphi_{10}\right)+c_{0910}\left(\dot{\varphi}_9-\dot{\varphi}_{10}\right)-R_{10}F_{\mathrm{R}}}{J_{10}},\\
\ddot{x}_{10} &= \frac{-k_{10x}\left(x_{10}-x_{10}'\right)-c_{10x}\left(\dot{x}_{10}-\dot{x}_{10}'\right)-(1/2)\cos\alpha_2 F_{\mathrm{R}}}{m_{10}},\\
\ddot{y}_{10} &= \frac{-k_{10y}\left(y_{10}-y_{10}'\right)-c_{10y}\left(\dot{y}_{10}-\dot{y}_{10}'\right)+k_{9y}\left(y_9-y_{10}\right)+c_{9y}\left(\dot{y}_9-\dot{y}_{10}\right)+(1/2)\sin\alpha_2 F_{\mathrm{R}}}{m_{10}},\\
\ddot{z}_{10} &= \frac{k_{9z}\left(z_9-z_{10}\right)+c_{9z}\left(\dot{z}_9-\dot{z}_{10}\right)-k_{10z}\left(z_{10}-z_{10}'\right)-c_{10z}\left(\dot{z}_{10}-\dot{z}_{10}'\right)}{m_{10}+m_{11}},\\
\ddot{x}_{11} &= \frac{-(1/2)\cos\alpha_2 F_{\mathrm{R}}-k_{11x}x_{11}-c_{11x}\dot{x}_{11}}{m_{11}},\\
\ddot{y}_{11} &= \frac{(1/2)\sin\alpha_2 F_{\mathrm{R}}-k_{11y}y_{11}-c_{11y}\dot{y}_{11}}{m_{11}},\\
\ddot{z}_{11} &= \frac{k_{9z}\left(z_9-z_{10}\right)+c_{9z}\left(\dot{z}_9-\dot{z}_{10}\right)-k_{10z}\left(z_{10}-z_{10}'\right)-c_{10z}\left(\dot{z}_{10}-\dot{z}_{10}'\right)}{\left(m_{10}+m_{11}\right)},\\
\ddot{u}_{12} &= \frac{\cos\alpha_1 F_{\mathrm{R}}+F\sin\gamma-k_{12u}u_{12}-c_{12u}\dot{u}_{12}}{m_{12}},\\
\ddot{v}_{12} &= \frac{(1/2)R_{12}^4\sin\alpha_1 F_{\mathrm{R}}-(1/2)FR_{12}^4\cos\gamma-(1/2)R_{12}^4 k_{12v}v_{12}-(1/2)R_{12}^4 c_{12v}\dot{v}_{12}}{J_{12}},
\end{aligned}
\tag{8}
$$

where J_{10} and J_{12} are the rotational inertia of the drum and the boom; m_{10}, m_{11} are half mass of drum; m_{12} is the boom mass; $x_{10}, z_{10}, x_{11}, y_{11}, z_{11}$ are displacements of node 10 and node 11; u_{12}, v_{12} are displacements of boom; $k_{10x}, k_{10z}, k_{11x}, k_{11y}, k_{11z}$ are stiffness of bearings; k_{12u}, k_{12v} are equivalent stiffness of the boom; $c_{10x}, c_{10z}, c_{11x}, c_{11y}, c_{11z}$ are dampings of bearings; c_{12u}, c_{12v} are equivalent dampings of the boom; R_{10} and R_{12} are the radii of drum and boom rotation; F is the force transformed from digger; α_1, α_2 are included angles of steel ropes to boom and ropes to horizontal; γ is the included angle of direction F and direction perpendicular to boom; and F_R is the force loading in steel rope which can be written as

$$\begin{aligned} F_R = {} & k_{1012}\left(\varphi_{10}R_{10} - v_{12}\sin\alpha - u_{12}\cos\alpha\right) \\ & + c_{1012}\left(\dot{\varphi}_{10}R_{10} - \dot{v}_{12}\sin\alpha - \dot{u}_{12}\cos\alpha\right). \end{aligned} \tag{9}$$

2.2. Dynamic Model of Control System. The EMS hoist motors are three phase asynchronous motor which is a high order, nonlinear system [20, 21]. Because of the advantages in reducing order and decoupling, the VC system has been used widely in various fields. The basic idea of VC is that after decoupling the stator excitation and torque by vector transformation, the flux and electromagnetic torque of the motor can be controlled independently [22], like speed control of DC motor.

In the VC system, the stator currents i_a, i_b, and i_c in three-phase coordinate system can be transformed to i_d and i_q in synchronous rotating reference frame by vector transformation. In M-T synchronous rotating reference frame, M axis is taken along the rotor total flux while T axis is perpendicular to it.

Rotor flux ψ_r, rotation speed error ω_s, and electromagnet torque T_e can be calculated as follows:

$$\psi_r = \frac{L_m}{T_r p + 1} i_{sM}, \tag{10}$$

$$\omega_s = \frac{L_m i_{sT}}{T_r \psi_r}, \tag{11}$$

$$T_e = n_p \frac{L_m}{L_r}\, pt i_{sT} \psi_r, \tag{12}$$

where L_m is common reactance; i_{sM}, i_{sT} are stator/rotor currents; ψ_r is rotor flux; and n_p is the number of pole pairs.

L_r is rotor self-inductance and T_r is rotor excitation time constant, which can be obtained by the following equation:

$$T_r = \frac{L_r}{R_r}, \tag{13}$$

where R_r is the rotor resistance.

Based on the mathematical model, the VC system is improved in Simulink/Matlab and shown in Figure 7. The current transformation and flux observation module is established with Equations (10) and (11) and shown in Figure 8. In current transformation and flux observation module, the rotor flux and rotational speed error can be calculated by the two-phase current after transformed. Then the control current i_{sM} can be obtained by the flux regulator using rotor flux error. At the same time, the rotational speed of M-T coordinate system can be calculated by rotational speed error and rotor speed. ASR and ATR are two PI controllers used to calculate the other current i_{sT}.

According to the VC system model, the electromagnet torque T_e can be simulated to drive the mechanical system.

3. Dynamic Results and Analysis

The main technical parameters of example EMS are listed in Table 1. Although people often ignore the torque ripple when analyzing the dynamic response, the electromagnet torque ripple widely exists. For closing to actual condition utmost, the ripple driving torque is simulated for analyzing the real dynamic response of hoist system.

3.1. Modal Property of Hoist System. Based on Equations (1), (3) and (8), the equivalent mathematic model of EMS hoist system can be derived as

$$\mathbf{M}\ddot{q}(t) + \mathbf{C}\dot{q}(t) + \mathbf{K}\mathbf{q}(t) = \mathbf{F}(t), \tag{14}$$

where $\mathbf{M}$ is mass matrix, $\mathbf{C}$ is damping matrix, $\mathbf{K}$ is stiffness matrix, $\mathbf{q}(t)$ is vibration displacement vector, and $\mathbf{F}(t)$ is the force vector.

According to the parameters listed in Tables 2 and 3, the natural frequencies and vibration modes of EMS hoist system can be calculated by Equation (14). The natural frequencies are listed in Table 4, and vibration modes are shown in Figure 9.

Based on the different component motion characteristics, the vibration modes can be classified to five types: rotational vibration mode, direction z vibration mode, x-y plane vibration mode, single-point vibration mode, and all freedoms vibration mode.

In rotational vibration mode, only motors and gears have rotational motion while other components are static. In direction z vibration mode, reducer shell, gears, and drum move along direction z, and the boom has no action. In x-y plane vibration mode, the components' motion is contrary to direction z vibration mode. Reducer shell, gears, drum, and boom move in all directions except direction z. There is only a single point moving along one direction in single-point vibration mode. Moreover, the only three same natural frequencies occur in this vibration mode. As for all freedoms vibration mode, all components have motion in every direction.

3.2. Dynamic Response of VC System. The hoist system usually suffers from shock loads as a result of inadequately blasted ores. To simulate impact working condition, an impact load curve is set as Figure 10. There is no load in startup step in first 0.5 s; then the hoist system works with

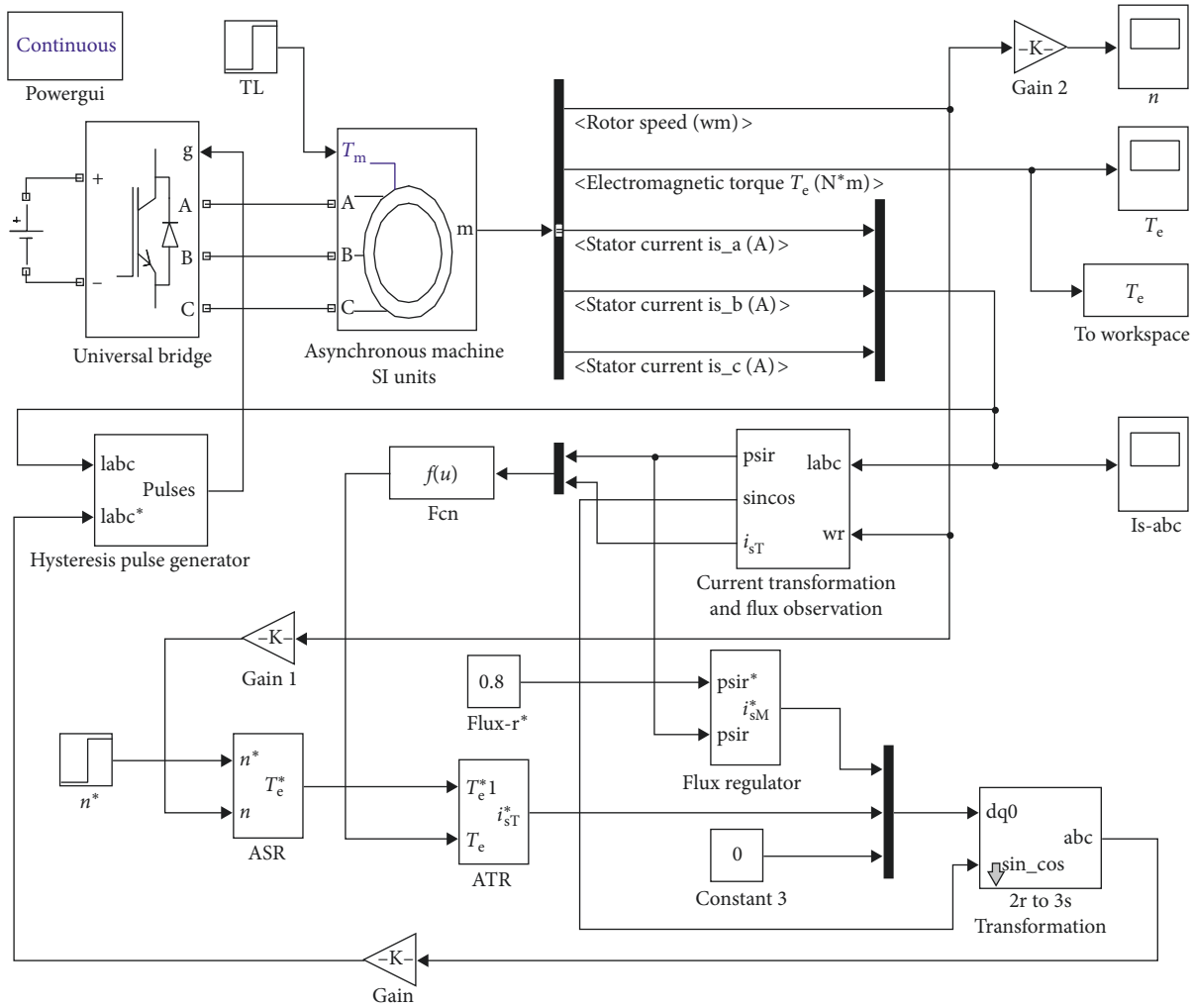

Figure 7: VC system of the EMS hoist motor.

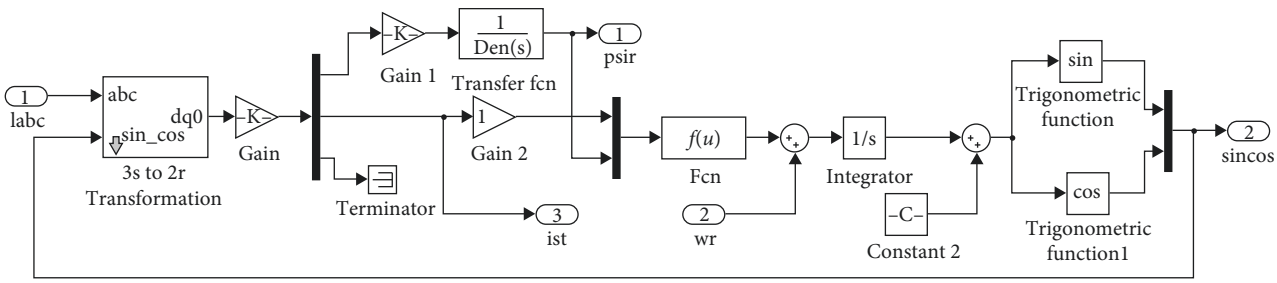

Figure 8: Current transformation and flux observation module.

rated load in 0.5 s to 5 s. However, there is a 0.5 times impact of rated load during 2 s to 3.5 s. The rated load can be calculated from

$$T_{\mathrm{m}} = 9550\frac{P_m}{n_{\mathrm{m}}}, \tag{15}$$

where T_{m} is the rated load of motor, P_m is the rated power, and n_{m} is the rated speed.

The concrete technical parameters of hoist motor are listed in Table 5. According to the simulation model, simulated speed and driving torque of hoist motor are shown in Figure 11.

In startup phase, driving torque rises to pull-in torque rapidly and rotational speed improves swiftly. After 0.2 s, rotational speed gets the rated speed, meanwhile driving torque turns to empty load and ripples around it. When the hoist motor works at rated and impact load, the driving torque is also rippling nearby corresponding load, and rotational speed maintains constant basically except has a little drop at the start of impact. The main frequencies of vibration

Table 1: Technical parameters of hoist system in EMS.

	Parameter	Value
Motor	Rated power	1115 kW
	Rated speed	473 r/min
Reducer	Decelerator ratio	50.865
	Shell mass	10,505 kg
Drum	Diameter	1.732 m
	Mass	22,810 kg
	Moment of inertia	9428 kg·m^2
Rope	Diameter	0.08 m
	Length	20 m
Boom	Mass	54,270 kg
	Moment of inertia	5,908,723 kg·m^2

Table 2: Transmission parameters of gear subsystem.

Parameter	1st		2nd	
	Drive gear	Driven gear	Drive gear	Driven gear
Tooth number, z	17	140	17	105
Mass, m (kg)	182	2688	912	9098
Moment of inertia, I (kg·m^2)	3.68	594.42	14.14	2602
Module, m_n	12		25	
Average mesh stiffness, k_0 (N/m)	19.5011×10^9		20.1119×10^9	
Coupling stiffness (N/m)	$k_y = 1 \times 10^{10}$		$k_z = 5 \times 10^{10}$	
Pressure angle, α (°)	20			

Table 3: Coupling stiffness of hoist system in EMS.

Coupling stiffness	x direction (N/m)	y direction (N/m)	z direction (N/m)	Rotational (N·m/rad)
Coupling, motor-gear	—	—	—	6×10^8
Bolt, reducer shell-ground	8×10^9	8×10^9	8×10^9	—
Bolt, gear-drum	—	1×10^{10}	5×10^{10}	2×10^9
Bering, gear-reducer shell	1×10^{10}	1×10^{10}	5×10^{10}	—
Bering, drum-reducer shell	1×10^{10}	1×10^{10}	5×10^{10}	—
Bering, drum-ground	1×10^{10}	1×10^{10}	5×10^{10}	—

Table 4: Natural frequencies and vibration modes.

Motion modes	Natural frequency (Hz)
Rotational vibration modes	$f_1 = 40$; $f_2 = 90$
Direction z vibration modes	$f_3 = 219$; $f_5 = 279$; $f_{20} = 2098$; $f_{21} = 2392$; $f_{28} = 4523$; $f_{29} = 5207$; $f_{37} = 16{,}304$; $f_{38} = 17{,}874$
x-y plane vibration modes	$f_4 = 236$; $f_6 = 376$; $f_7 = 418$; $f_8 = 436$; $f_9 = 572$; $f_{10} = 934$; $f_{14} = 1096$; $f_{15} = 1280$; $f_{19} = 2003$; $f_{22} = 2623$; $f_{31} = 7514$; $f_{32} = 7548$; $f_{33} = 10{,}254$; $f_{34} = 11{,}033$
Single-point vibration modes	$f_{11} = f_{12} = f_{13} = 936$; $f_{16} = 1510$; $f_{24} = 3534$; $f_{25} = 3911$; $f_{30} = 7084$
All freedoms vibration modes	$f_{17} = 1613$; $f_{18} = 1714$; $f_{23} = 3333$; $f_{26} = 3974$; $f_{27} = 4006$; $f_{35} = 15{,}097$; $f_{36} = 15{,}457$

torque are 147.6 Hz and 297.5 Hz, marked as f_{dm} and $2f_{dm}$ in Figure 11(c). Between 2nd and 5th order natural frequency, the ripple torque may cause system resonance.

3.3. Dynamic Analysis in Time Domain. According to the parameters in Table 2, the time-varying stiffness and mesh error can be calculated and shown in Figures 12 and 13.

The dynamic response of hoist system can be calculated with the Runge–Kutta method in Matlab software under the simulated driving torque showed in Figure 11(b). The vibration displacements and accelerations of reducer shell, 2nd drive gear, and drum are shown in Figure 14.

For the general vibration displacement trend, reducer shell, 2nd drive gear, and drum are the same. During the

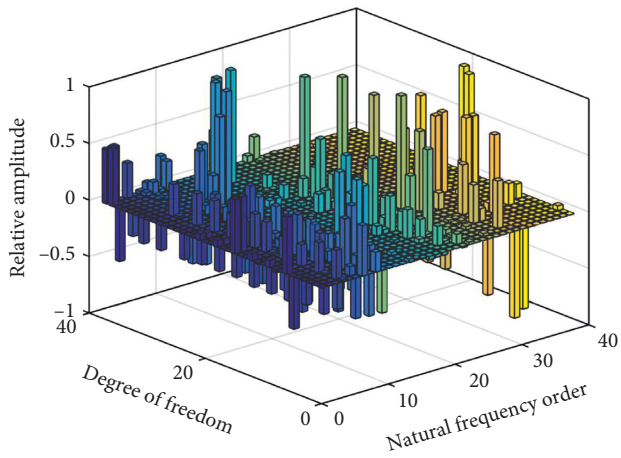

Figure 9: Vibration modes of EMS hoist system.

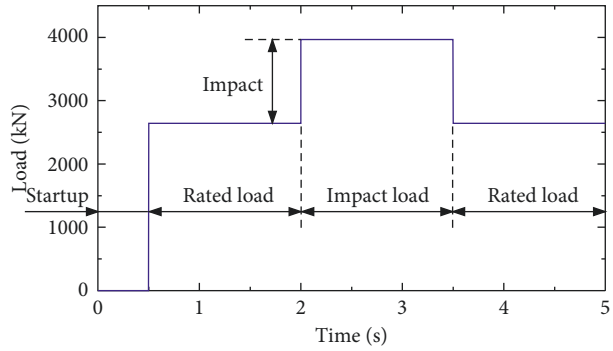

Figure 10: Impact load curve.

Table 5: Parameters of driving motor.

Parameters	Value
Rated voltage U_N	690 V
Rated frequency f_N	24 Hz
Stator resistance R_s	0.008 Ω
Rotor resistance R_r	0.018 Ω
Stator inductance L_s	0.016 mH

first 0.2 s, the displacements rise up quickly and reach a peak. Then, the amplitudes start reducing in the next 0.3 s because the electromagnetic torque drops to zero. The displacements wave around zero axis after transition stage. When the load increases to 1.5 times of its rated value, the vibration amplitudes are also increased to 1.5 times of its previous value. After the impact disappears, the displacements turn back to before impact. That is, the vibration displacements are not related to the previous vibration. Contrasting Figures 14(a), 14(c), and 14(e), the amplitudes under stable vibration become large from reducer shell to drum. Therefore, the vibration is amplified with the force transmission.

The vibration acceleration of reducer shell is similar to 2nd drive gear. Along the change of load, the acceleration amplitudes also change as the same proportion. Meanwhile, the drum vibration amplitude is also proportional to the load. In Figure 14(f), the drum has acceleration mutations because the rope force loaded on the drum directly has abrupt changes along the load changing.

3.4. Dynamic Analysis in Frequency Domain. In order to research the dynamic response further, the acceleration responses of reducer shell, 2nd drive gear, and drum in frequency domain curves are plotted in Figure 15. The mesh frequency, shaft frequency of gear subsystem, and motor torque frequency are listed in Table 6.

The main frequencies of reducer shell, 2nd drive gear, and drum are mesh frequencies and their frequencies doubling. But the lower frequencies which are related to 2nd mesh frequency have some differences between them. The number of lower frequencies covers from less to more in reducer shell, 2nd drive gear, and drum. So, the coupled vibration in executive end is more complex than drive end.

Of equal importance, the vibration acceleration frequencies contain motor torque frequencies (f_{dm}, $2f_{dm}$) in reducer shell and 2nd drive gear. That is, motor torque ripple has influence to the system vibration. Although the amplitudes in f_{dm} and $2f_{dm}$ are little, we cannot

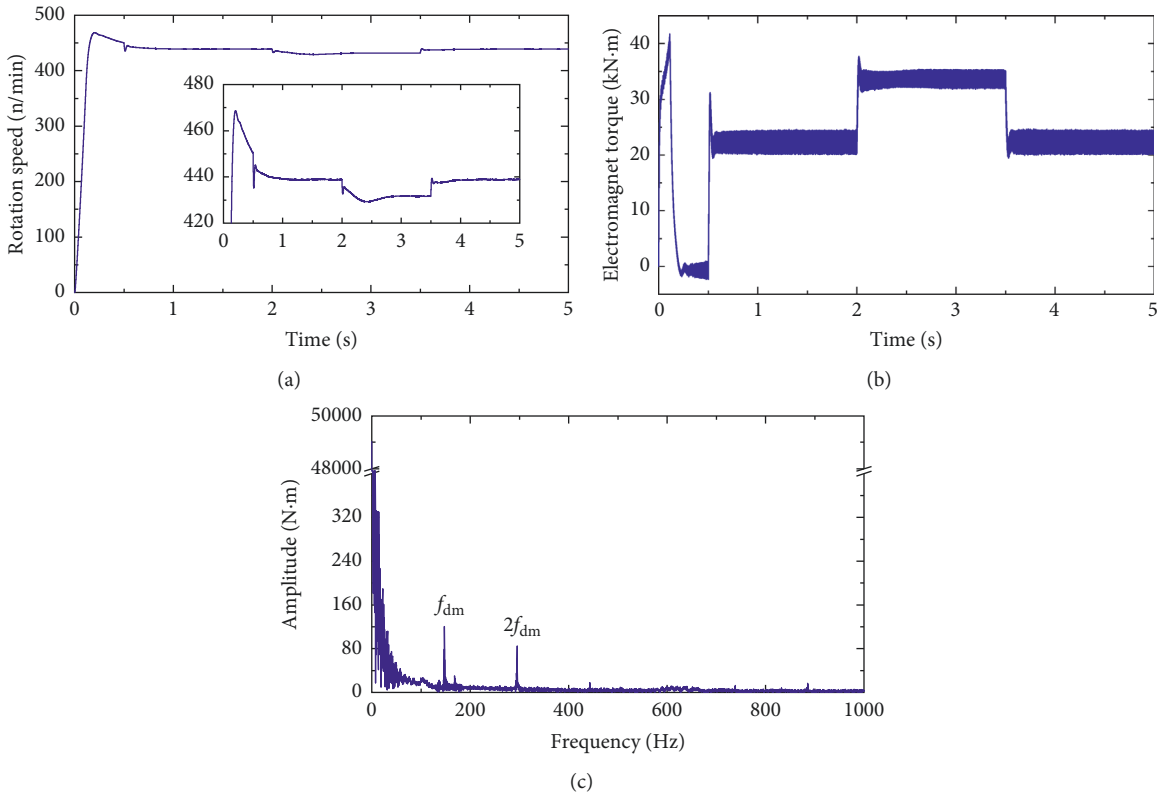

Figure 11: Simulated results of hoist motor. (a) Rotational speed. (b) Driving torque. (c) Frequency-domain curve of driving torque.

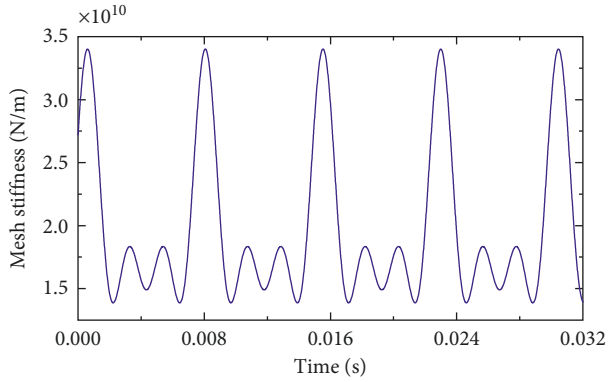

Figure 12: Mesh stiffness of gear 3 and gear 4.

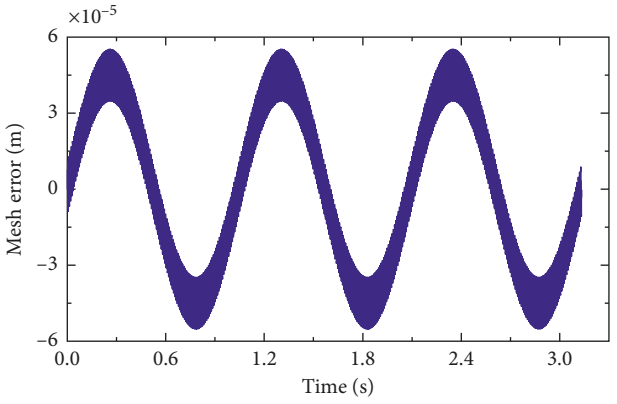

Figure 13: Mesh error of gear 3 and gear 4.

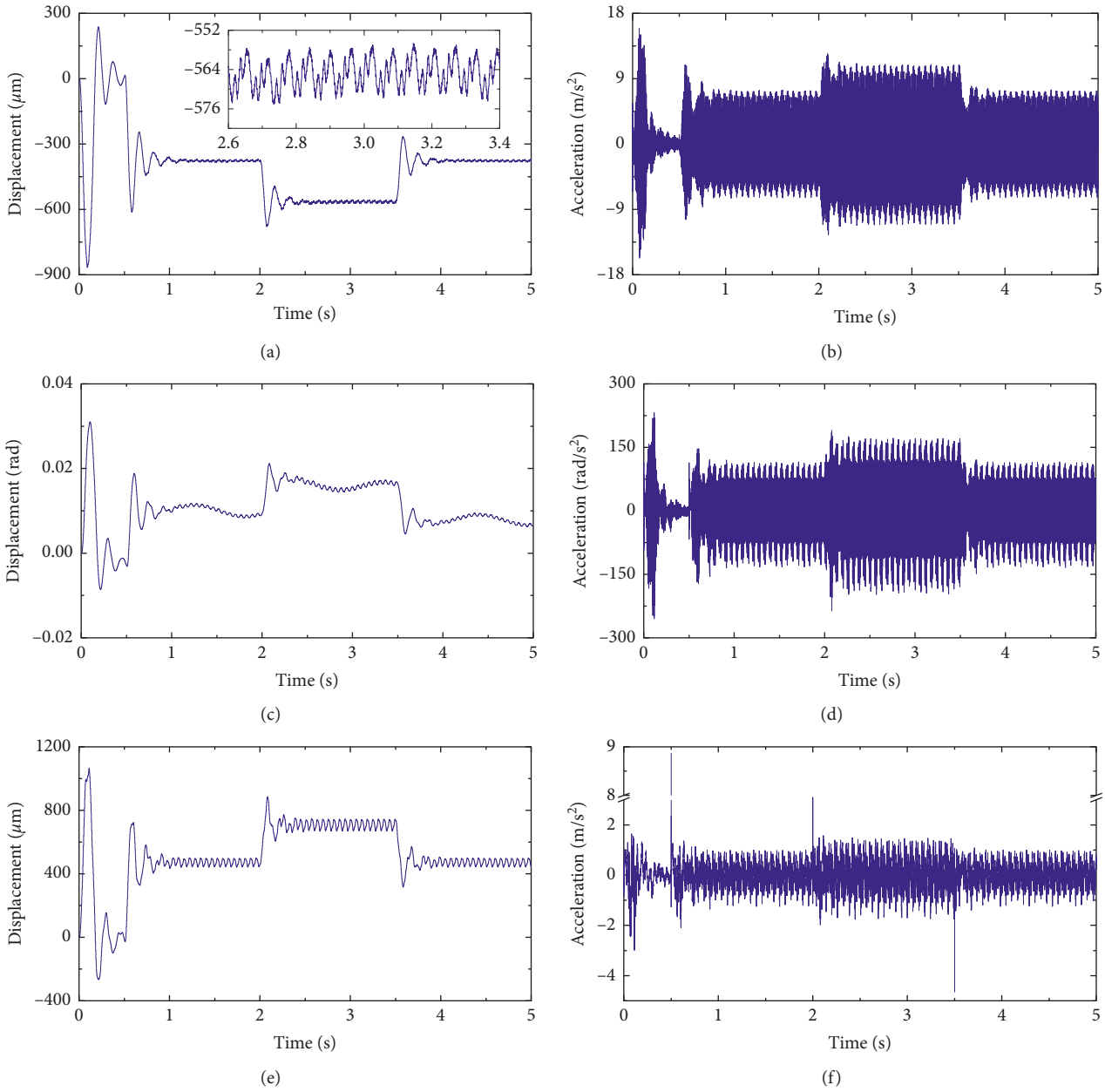

Figure 14: Vibration displacements and accelerations. (a) Reducer shell displacement in direction y. (b) Reducer shell acceleration in direction y. (c) 2nd drive gear angular displacement. (d) 2nd drive gear angular acceleration. (e) Drum displacement in direction y. (f) Drum acceleration in direction y.

neglect it. If the motor control system could not be set reasonably or suffers failure, the ripple torque amplitude may get larger and may have a big impact to the whole system.

3.5. Model Verification. For analyzing the vibration of EMS hoist system, the manufacturer tested the vibration of reducer shell under rated load. The actual test field and measuring point positions are shown in Figure 16.

The test results in time domain are shown in Figure 17. Similar to the model responses in rated load, the vibration of reducer shell is regular in 130 to 140 s. The concrete data of model responses and test results are listed in Table 7.

The relative errors of average amplitude are below 30% whether point 2 or point 4. However, the relative errors of root amplitude are over 30%. That is, the actual amplitude fluctuation is larger than ideal situation. It is mainly caused by the vibration of reducer platform, manufacturing, and installation error. Therefore, the model responses are reliable in time domain [23, 24].

The comparison of point 2 acceleration vibration in frequency domain is shown in Figure 18. The main

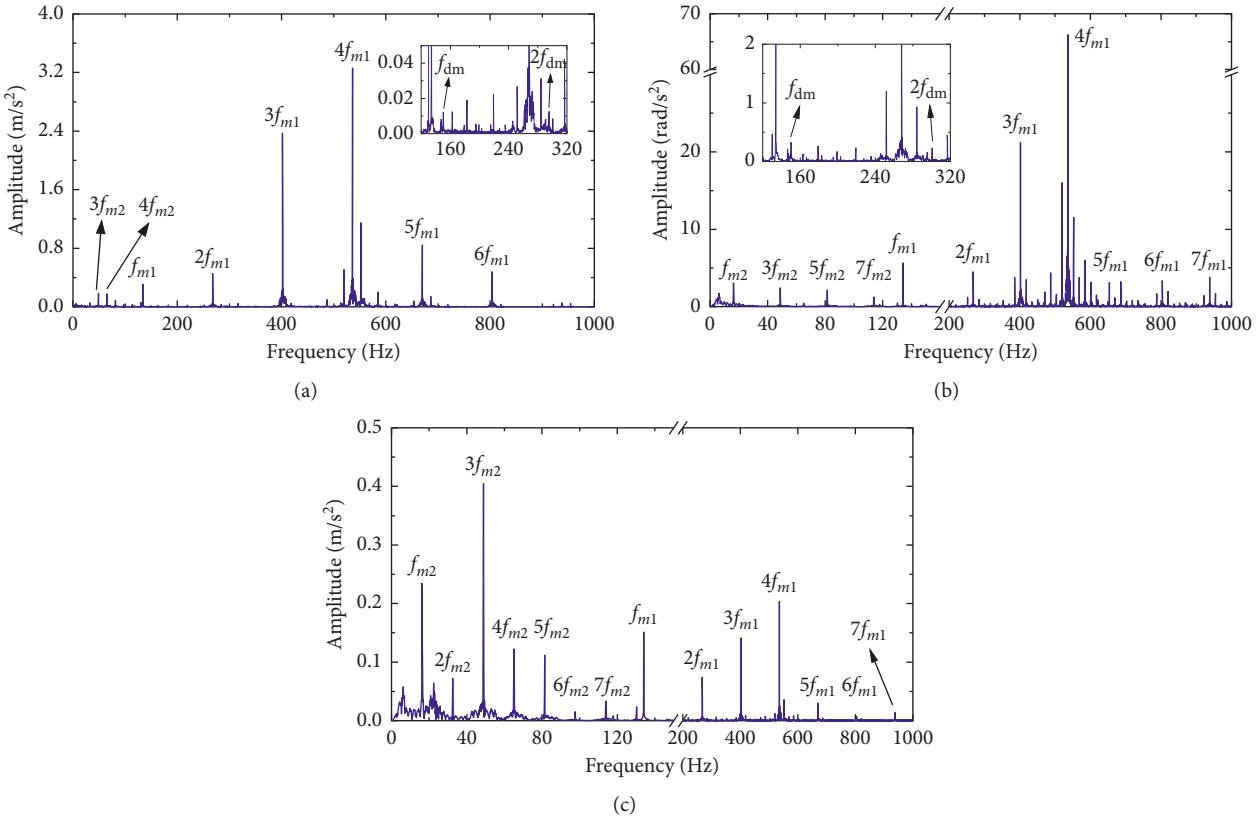

Figure 15: Frequency-domain curves of acceleration. (a) Reducer shell in direction y. (b) 2nd drive gear in rotational direction. (c) Drum in direction y.

Table 6: Excitation frequency of gear subsystem and motor.

Parameter			Value
Motor speed (r/min)		—	473
Motor frequency		f_{dm}	147.6
Mesh frequency (Hz)	1st	f_{m1}	134.0
	2nd	f_{m2}	16.3
Shaft frequency (Hz)	Input shaft	f_{s1}	7.9
	Intermediate shaft	f_{s2}	1.0
	Output shaft	f_{s3}	0.2

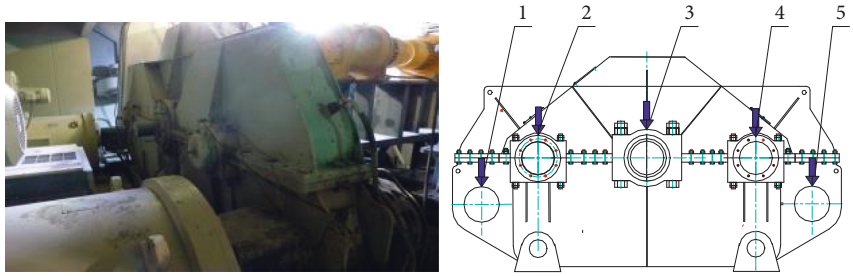

Figure 16: Actual field and measuring point positions.

frequencies of test vibration are three times of 2nd mesh frequency and frequencies doubling of 1st mesh frequency. Accordingly, the vibration frequency properties are the same in test and model, which are frequencies doubling of mesh frequency. Consequently, the model responses are also reliable in frequency domain.

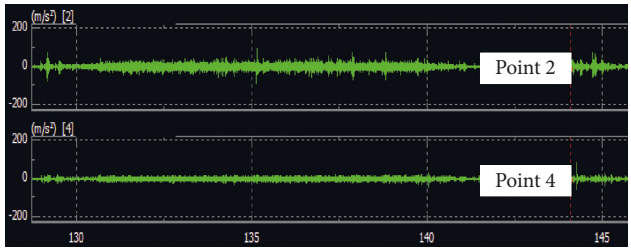

Figure 17: Test results in time domain.

Table 7: Data comparison of test and model.

Acceleration in direction y (m/s^2)		Test	Model	Relative error (%)
Point 2	Average amplitude	5.65	4.17	26.2
	Root amplitude	4.37	2.31	47.1
Point 4	Average amplitude	3.43	3.33	2.9
	Root amplitude	2.71	1.85	31.7

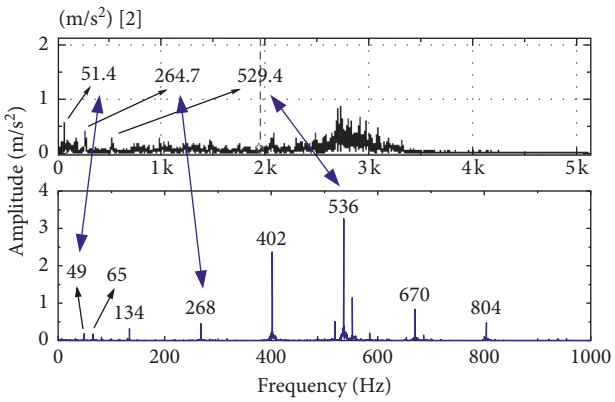

Figure 18: Frequency comparison of point 2.

4. Conclusions

(1) A coupled dynamic model including mechanical and control system is presented and verified using hierarchical modeling way. The modeling process can provide some reference to modeling of other complex equipment.

(2) Based on the dynamic analysis of the hoist system, vibration modes can be classified to five types: rotational vibration mode, direction z vibration mode, x-y plane vibration mode, single-point vibration mode, and all freedoms vibration mode.

(3) The vibration displacements amplitude and equilibrium position are proportional to load while the vibration accelerations amplitude are also proportional to load. The vibration frequencies are main mesh frequencies and their frequencies doubling. From drive end to executive end, the vibration amplitudes get larger and larger, and coupled frequencies are more and more complex as well.

(4) There are motor torque frequencies in vibration accelerations, and the ripple torque may cause system resonance. This can explain that motor torque vibration has affection to the vibration of the whole system.

Data Availability

The data used to support the findings of this study are currently under embargo, while the research findings are commercialized. Requests for data, 6 months after publication of this article, will be considered by the corresponding author.

Conflicts of Interest

The authors declare no potential conflicts of interest with respect to the research, authorship, and/or publication of this article.

Acknowledgments

This work was supported by the National Natural Science Foundation of China (51605071 and U1608256) and the Special Grade of the China Postdoctoral Science Foundation (2016T90218).

References

[1] R. G. Parker, S. M. Vijayakar, and T. Imajo, "Non-linear dynamic response of a spur gear pair: modeling and experimental comparisons," *Journal of Sound and Vibration*, vol. 237, no. 3, pp. 435–455, 2000.

[2] K. Awuah-Offei and S. Frimpong, "Numerical simulation of cable shovel resistive forces in oil sands excavation," *International Journal of Mining, Reclamation and Environment*, vol. 20, no. 3, pp. 223–238, 2006.

[3] A. Rasuli, S. Tafazoli, and W. G. Dunford, "Dynamic modeling, parameter identification, and payload estimation of mining cable shovels," in *Proceedings of IEEE Conference on Industry Applications Society Annual Meeting*, pp. 1–9, Vancouver, Canada, October 2014.

[4] K. Awuah-Offei and S. Frimpong, "Efficient Cable shovel excavation in surface mines," *Geotechnical and Geological Engineering*, vol. 29, no. 1, pp. 19–26, 2011.

[5] J. Huo, H. Wu, G. Li, W. Sun, and J. Chen, "The coupling dynamic analysis and field test of TBM main system under multipoint impact excitation," *Shock and Vibration*, vol. 2015, Article ID 313259, 14 pages, 2015.

[6] J. Zhang, Q. Chao, B. Xu et al., "Novel three-piston pump design for a slipper test rig," *Applied Mathematical Modelling*, vol. 52, pp. 65–81, 2017.

[7] L. Li, D. Kong, Y. Lin et al., "Simulation study on performance of hoist mechanism of electric mining shovel," *Coal Mine Machinery*, vol. 32, pp. 82–85, 2011, Chinese.

[8] M. B. Khorzoughi and R. Hall, "Application of vibration analysis of mining shovels for diggability assessment in open-pit operations," *International Journal of Mining, Reclamation and Environment*, vol. 29, no. 5, pp. 380–390, 2015.

[9] M. V. Guzmán and M. A. Valenzuela, "Integrated mechanical-electrical modeling of an AC electric mining shovel and evaluation of power requirements during a truck

loading cycle," in *Proceedings of 2014 IEEE Industry Application Society Annual Meeting*, pp. 2590–2599, Vancouver, Canada, October 2015.

[10] J. Wei, Q. Sun, W. Sun, X. Ding, W. Tu, and Q. Wang, "Load-sharing characteristic of multiple pinions driving in tunneling boring machine," *Chinese Journal of Mechanical Engineering*, vol. 26, no. 3, pp. 532–540, 2013.

[11] J. Wei, Q. Sun, W. Sun et al., "Dynamic analysis and load-sharing characteristic of multiple pinion drives in tunnel boring machine," *Journal of Mechanical Science and Technology*, vol. 27, no. 5, pp. 1385–1392, 2013.

[12] D. Qin, J. Wang, and T. C. Lim, "Flexible multibody dynamic modeling of a horizontal wind turbine drivetrain system," *Journal of Mechanical Design*, vol. 131, no. 11, pp. 1–8, 2009.

[13] W. Sun, H. Ma, X. Song, L. Wang, and X. Ding, "Modeling and dynamic analysis of cutterhead driving system in tunnel boring machine," *Shock and Vibration*, vol. 2017, Article ID 7156816, 12 pages, 2017.

[14] W. Sun, X. Ding, J. Wei, X. Wang, and A. Zhang, "Hierarchical modeling method and dynamic characteristics of cutterhead driving system in tunneling boring machine," *Tunnelling and Underground Space Technology*, vol. 52, pp. 99–110, 2016.

[15] J. Zhang, M. Yang, B. Xu, R. Ding, M. Cheng, and P. Dong, "A novel intelligent sliding sleeve for shale oil and gas mining equipment," *Journal of Petroleum Science and Engineering*, vol. 158, pp. 1–10, 2017.

[16] R. Li and J. Wang, *Gear System Dynamic*, SciencePress, Beijing, China, 1996, Chinese

[17] R. G. Parker and J. Lin, "Mesh phasing relationships in planetary and epicyclic gears," *Journal of Mechanical Design*, vol. 126, no. 2, pp. 365–370, 2004.

[18] J. D. Smith, *Gear Noise and Vibration*, CRC Press, New York, NY, USA, 2003.

[19] A. Kahraman, "Load sharing characteristics of planetary transmissions," *Mechanism and Machine Theory*, vol. 29, no. 8, pp. 1151–1165, 1994.

[20] C. Zhang, G. Wu, F. Rong et al., "Robust fault-tolerant predictive current control for permanent magnet synchronous motors considering demagnetization fault," *IEEE Transactions on Industrial Electronics*, vol. 65, no. 7, pp. 5324–5334, 2018.

[21] P. Kakosimos and H. Abu-Rub, "Predictive speed control with short prediction horizon for permanent magnet synchronous motor drives," *IEEE Transactions on Power Electronics*, vol. 33, no. 3, pp. 2740–2750, 2018.

[22] J. W. Jung, Y. S. Choi, V. Q. Leu et al., "Fuzzy PI-type current controllers for permanent magnet synchronous motors," *IET Electric Power Applications*, vol. 5, no. 1, pp. 143–152, 2001.

[23] S. Hu, C. Ma, J. Yang et al., "Investigation into effect of thermal expansion on thermally induced error of ball screw feed drive system of precision machine tools," *International Journal of Machine Tools and Manufacture*, vol. 97, pp. 60–71, 2015.

[24] S. Hu, D. Zhang, J. Yang et al., "Experiment-based thermal error modeling method for dual ball screw feed system of precision machine tool," *International Journal of Advanced Manufacturing Technology*, vol. 82, no. 9–12, pp. 1693–1705, 2016.